THE ASTRONOMICAL JOURNAL VOLUME 106, NUMBER 6 DECEMBER 1993

# THE CIRCUMSTELLAR ENVIRONMENT OF THE FU ORIONIS PRE-OUTBURST CANDIDATE V1331 CYGNI

STUART MCMULDROCH

Division of Geological and Planetary Sciences, 170-25, California Institute of Technology, Pasadena, California 91125
Electronic mail: sxm@sol1.gps.caltech.edu

ANNEILA I. SARGENT

Division of Physics, Mathematics, and Astronomy, California Institute of Technology, 105-24, Pasadena, California 91125
Electronic mail: afs@mmstar.caltech.edu

GEOFFREY A. BLAKE

Division of Geological and Planetary Sciences, 170-25, California Institute of Technology, Pasadena, California 91125
Electronic mail: gab@csardas.gps.caltech.edu

*Received 1993 July 14*

## ABSTRACT

High resolution ($\sim 4''$) aperture synthesis maps of the CO (1→0), $^{13}$CO (1→0), $^{13}$CO (2→1), and associated continuum emission from the FU Orionis candidate V1331 Cygni reveal a massive, $0.5 \pm 0.15 \mathcal{M}_\odot$, circumstellar disk surrounded by a flattened gaseous envelope, $6000 \times 4400$ AU in size, mass $\geqslant 0.32 \mathcal{M}_\odot$. These images and lower resolution measurements also trace a bipolar outflow and gaseous ring, 4.1 by $2.8 \times 10^4$ AU, mass $\geqslant 0.07 \mathcal{M}_\odot$, radially expanding at $22 \pm 4$ km s$^{-1}$. We suggest this ring is a swept-up gaseous torus from an energetic mass ejection stage, possibly an FU Orionis outburst or outbursts, $\sim 4 \times 10^3$ yr ago that imparted $\geqslant 10^{45}$ ergs into the ambient cloud.

## 1. INTRODUCTION

Beginning in 1936, FU Orionis, a little-studied star in Orion, rose in brightness from about $16^m$ to $10^m$ over a period of half a year (Wachmann 1939). Since then, several other stars have exhibited similar behavior, most notably V1057 Cygni. These FU Orionis objects (FUors) have distinctive spectral signatures; their Balmer lines exhibit P Cygni profiles with a suppressed emission component, while absorption linewidths and spectral type varies with wavelength and often show a double-peaked structure (Herbig 1977, 1989; Hartmann & Kenyon 1987; Reipurth 1990; Petrov & Herbig 1992; Welty *et al.* 1992; Hartmann *et al.* 1993). Several stars have been classified as FUors based solely on their spectra (Mundt *et al.* 1985; Carr *et al.* 1987; Eislöffel *et al.* 1990; Staude & Neckel 1991).

Pioneering work by Hartmann & Kenyon (1985, 1987) explains many of the observed properties of FUors in terms of accretion through a circumstellar disk onto a T Tauri star, outbursts result when the disk becomes unstable producing an elevated accretion rate (see also Calvet *et al.* 1991; Hartmann 1992; Hartmann *et al.* 1993). For a few objects, optical and near-infrared spectral line profiles suggest that the disk material moves in Keplerian orbits (Hartmann & Kenyon 1987; Welty *et al.* 1992). Little is known about the pre-outburst nature of FUors, although a pre-outburst spectrogram of V1057 Cygni identifies it as a strong-lined T Tauri star (Herbig 1958). The frequency of detected FUor eruptions indicates that a T Tauri star undergoes up to 100 outbursts, although this conclusion is based on small sample statistics (Herbig 1977, 1989; Hartmann 1992).

V1331 Cygni is a luminous ($\sim 53 L_\odot$) T Tauri star, visual extinction $A_v \sim 2.4$, at a distance of 550 pc (Shevchenko *et al.* 1991). Although other distances have been adopted, here all properties are scaled to 550 pc. The similarity of the spectrum of V1331 Cygni to that of V1057 Cygni prior to maximum light, with the K line of Ca II (3933 Å) strong in emission and the H line (3968 Å) absent, may signify an impending Fuor outburst (Welin 1976; Herbig 1989). Optical emission line profiles imply a moderate mass loss rate of $7 \times 10^{-8} \mathcal{M}_\odot$ yr$^{-1}$ to $3 \times 10^{-6} \mathcal{M}_\odot$ yr$^{-1}$, much less than the large rates exhibited by FUors of $\sim 10^{-5} \mathcal{M}_\odot$ yr$^{-1}$ (Chavarria 1981; Croswell *et al.* 1987). There is also evidence for a molecular outflow with a mass loss rate of $1.0 \times 10^{-7} \mathcal{M}_\odot$ yr$^{-1}$ (Levreault 1988). Submillimeter continuum observations suggest the presence of a circumstellar disk (Weintraub *et al.* 1991).

If V1331 Cygni is indeed a pre-outburst, or between outbursts, FUor, its circumstellar environment may retain some record of a previous event. The dramatic heating of a FUor outburst could, for example, result in an unusual chemical environment, or the increased mass loss episode may be reflected in the kinematics of the circumstellar gas. Here we present high resolution ($2''.2$–$5''.9$) aperture synthesis maps of V1331 Cygni in the CO (1→0), $^{13}$CO (1→0), and $^{13}$CO (2→1) transitions, along with measurements of the dust continuum emission at $\lambda = 1.3$ and $\lambda = 2.6$ mm. These observations trace the small scale density and temperature fluctuations in the circumstellar gas and dust. We have also acquired single dish observations of

 0004-6256/93/106(6)/2477/9/$0.90 

several isotopic forms of CO to determine optical depths and have mapped the CO (2→1) emission at ~30″ resolution to image the larger scale circumstellar environment.

## 2. OBSERVATIONS

### *2.1 Owens Valley*

Aperture synthesis mapping of the $J=1\rightarrow0$ rotational transitions of $^{12}CO$ and $^{13}CO$, as well as the $J=2\rightarrow1$ transition of $^{13}CO$ at $\nu=115.271$, 110.201, and 220.399 GHz, was carried out using the Owens Valley millimeter-wave interferometer between 1990, October and 1991, June. Each of the three 10.4 m diameter telescopes was equipped with a SIS receiver, cryogenically cooled to 4 K. System temperatures were typically 390 K (SSB) at 110 GHz, 850 K (SSB) at 115 GHz, and 740 K (SSB) at 220 GHz. Two filter banks, 32×1 MHz and 32×50 kHz, each centered on the CO velocity in the direction of the star, $v_{LSR}=-0.7$ km s$^{-1}$ (Levreault 1985), provided velocity resolutions of 2.7 and 0.14 km s$^{-1}$, 2.6 and 0.13 km s$^{-1}$, and 1.3 and 0.07 km s$^{-1}$ at 110.201, 115.271, and 220.399 GHz, respectively. Simultaneous continuum observations were obtained in a broadband channel of effective width 375 MHz, centered on the systemic velocity.

The phase and amplitude gains were calibrated by observing the quasar BL Lac at 25 min intervals, and the absolute flux scale was established by measurements of Neptune and Uranus. Maps were generated from calibrated visibility data using the NRAO AIPS software package. Positional accuracy is ±2″. At 110.201 and 220.339 GHz, maximum unprojected baselines of 140 m north–south and 200 m east–west gave naturally weighted synthesized beams of 4″.4×4″.1 at PA −30° and 3″.6×2″.3 at PA −25°. At 115.271 GHz, maximum baselines of 100 m north–south and 100 m east–west resulted in a naturally weighted beam of 5″.9×5″.2 at PA −5°. For these beams, $T_B=1$ K corresponds to 0.18, 0.32, and 0.33 Jy/beam respectively. The phase center of the maps is $\alpha$ (1950) $=20^h59^m32.21^s$, $\delta$ (1950) $=+50°09'55''.5$, the position of V1331 Cygni given by Herbig & Robbin Bell (1988).

### *2.2 CSO Observations*

Single dish observations were carried out at the Caltech Submillimeter Observatory (CSO) on Mauna Kea, Hawaii, in 1991, June and 1992, August. The facility 230 and 345 GHz SIS heterodyne receivers were used in conjunction with the CSO 500 and 50 MHz bandwidth acousto-optical spectrometers (Ellison & Miller 1987; Ellison *et al.* 1989). Calibration was accomplished by the standard chopper wheel method, while main beam efficiencies were calculated to ~20% from measurements of Jupiter. At 230 and 345 GHz, the beamwidths were 31″ and 21″ (FWHM), with main beam efficiencies of 0.52 and 0.58, respectively.

Although a number of molecular species were searched for in the 230 GHz band, only CO and its isotopes were detected toward V1331 Cygni to a 2$\sigma$ rms noise limit of ~180 mK. Spectra were acquired for the $J=2\rightarrow1$ rotational transitions of CO, $^{13}CO$, and $C^{18}O$, as well as the CO $J=3\rightarrow2$ transition. In addition, CO (2→1) emission was mapped on a 150″×150″ grid, sampled every 10″, centered on V1331 Cygni. Position switching to a reference position at $\alpha=20^h56^m43^s$, $\delta=+50°09'55''.5$ produced the least contaminated baselines. Pointing was checked regularly on planets and nearby point sources; absolute positions are accurate to within 5″, relative positions within the maps to ~2″.

## 3. RESULTS

### *3.1 Owens Valley Results*

Dust continuum emission from V1331 Cygni is unresolved in the 3″.6×2″.2 beam at 1.3 mm, indicating a source size less than 2000 AU. Emission appears centered on the star with fluxes of 33 mJy at 2.7 mm and 175 mJy at 1.3 mm.

Figures 1(a) and 1(b) show the CO (1→0) and $^{13}CO$ (1→0) emission from V1331 Cygni in the 50 kHz channels integrated over the velocity ranges −0.84 to +0.74 km s$^{-1}$ and −0.97 to +0.25 km s$^{-1}$ ($V_{LSR}$), respectively. No flux was detected outside these velocity ranges to 3$\sigma$ limits of 1.5 and 0.15 Jy/beam for CO and $^{13}CO$, respectively. The $^{13}CO$ (2→1) emission integrated between −1.21 and +0.12 km s$^{-1}$ is shown in Fig. 1(c). No emission was detected outside this velocity range to a 3$\sigma$ limit of 0.9 Jy/beam. All emission regions appear extended with deconvolved source sizes of 5500×2750, 6050×4400, and 2750×2200 AU for CO (1→0), $^{13}CO$ (1→0), and $^{13}CO$ (2→1). Within the positional uncertainties, emission in each transition peaks at the star.

The total integrated fluxes for the emission regions depicted in Fig. 1(a)–1(c), are 17, 8, and 22 Jy km s$^{-1}$. Following Scoville *et al.* (1986), the mass of $H_2$ implied in each case is given by

$$\mathcal{M}_{H_2}=2.19\times10^{-9}\times\frac{(T_x+0.93)}{e^{-5.53/T_x}}\frac{\tau_{CO}}{(1-e^{-\tau})}\frac{D^2_{kpc}}{X(CO)}\int S_\nu\,dv\;\mathcal{M}_\odot, \quad (1)$$

$$\mathcal{M}_{H_2}=2.39\times10^{-9}\times\frac{(T_x+0.89)}{e^{-5.31/T_x}}\frac{\tau_{^{13}CO}}{(1-e^{-\tau})}\frac{D^2_{kpc}}{X(^{13}CO)}\int S_\nu\,dv\;\mathcal{M}_\odot, \quad (2)$$

$$\mathcal{M}_{H_2}=1.71\times10^{-10}\times\frac{(T_x+0.89)}{e^{-15.92/T_x}}\frac{\tau_{^{13}CO}}{(1-e^{-\tau})}\frac{D^2_{kpc}}{X(^{13}CO)}\int S_\nu\,dv\;\mathcal{M}_\odot, \quad (3)$$

where Eqs. (1)–(3) are appropriate for CO (1→0), $^{13}CO$ (1→0), and $^{13}CO$ (2→1) line emission, respectively. Here $T_x$ is the excitation temperature, $\tau$ is the optical depth determined from line intensity ratios, $D$ is the source distance in kiloparsecs, $X$ is the molecular abundance relative

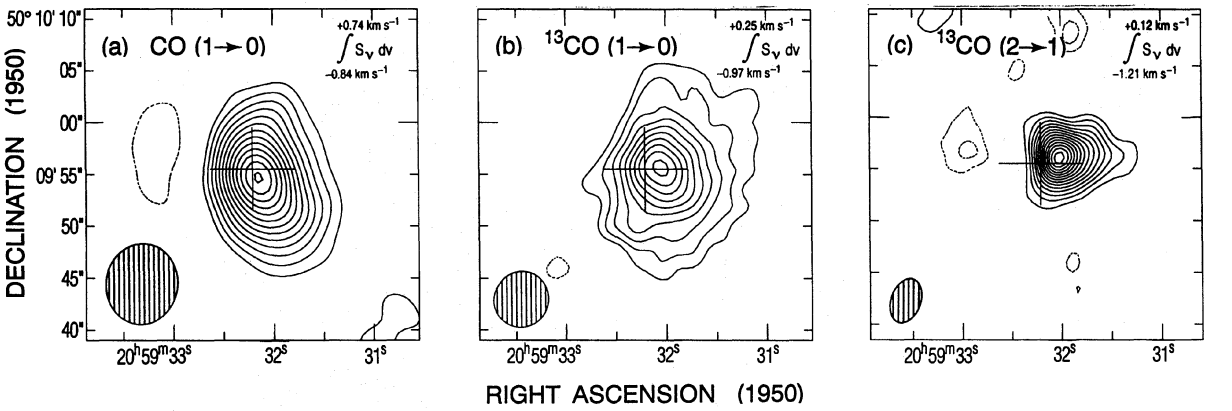


FIG. 1. (a) A map of the CO (1→0) emission integrated between $V_{LSR} = -0.84$ to $+0.74$ km s$^{-1}$. Contours start at the $2\sigma$ level, 1.0 Jy/beam km s$^{-1}$, and are separated by 0.50 Jy/beam km s$^{-1}$ ($1\sigma$). In all maps, a hatched ellipse denotes the synthesized beam (FWHM), and a cross, 8″ in size, marks the position of the star (Herbig & Robbin Bell 1988). (b) A map of the $^{13}$CO (1→0) emission around V1331 Cygni integrated between $-0.97$ to $+0.25$ km s$^{-1}$. Contours are separated by $1\sigma$, 0.15 Jy/beam km s$^{-1}$, starting at 0.30 Jy/beam km s$^{-1}$. (c) A map of $^{13}$CO (2→1) emission integrated between velocities $-1.21$ to $+0.12$ km s$^{-1}$. Contours begin at the $2\sigma$ value, 1.0 Jy/beam km s$^{-1}$, and are spaced by 0.50 Jy/beam km s$^{-1}$.

to hydrogen, and $\int S_\nu\, dv$ is the integrated flux in units of Jy km s$^{-1}$. We adopt abundances of $X(\mathrm{CO}) = 10^{-4}$, $X(^{13}\mathrm{CO}) = 1.7 \times 10^{-6}$ (Chackerian & Tipping 1983; Langer & Penzias 1993) and assume that the excitation temperature, as approximated by the kinetic temperature, is 25 K. For these values, the calculation is relatively insensitive to temperature—a 5 K difference corresponds to an ~20% change in mass. As all lines are optically thick, mass estimates are lower limits only. We calculate minimum masses of 0.32, 0.18, and 0.05$\mathscr{M}_\odot$ for CO (1→0), $^{13}$CO (1→0), and $^{13}$CO (2→1), respectively. This implies a minimum average density of $n_{H_2} \geqslant 3 \times 10^5$ cm$^{-3}$ for these masses and source sizes.

Naturally weighted, 1 MHz channel maps of the CO (1→0) emission from V1331 Cygni between $-9.8$ km s$^{-1}$ and $+11.0$ km s$^{-1}$ are presented in Fig. 2. Outside this velocity range, no emission above a $3\sigma$ limit of 135 mJy/beam is seen. Near the stellar position, emission is evident from $-2.0$ to $+11.0$ km s$^{-1}$. At distances of up to 50″, two elongated structures extend radially away from the star, concentrated toward PA $-25°$ and 230°. To the northwest, emission is seen between $-7.2$ and $-4.6$ km s$^{-1}$, to the southwest between $+0.6$ to $+8.4$ km s$^{-1}$.

Contours of the CO (1→0) emission, integrated between velocities of $-11.1$ to $-3.3$ km s$^{-1}$, are shown in Fig. 3(a). A greyscale image of this emission is also shown in Fig. 3(b) together with contours of the CO (1→0) emission at velocities between $+1.9$ to $+7.1$ km s$^{-1}$. The greyscale image in Fig. 3(a), kindly obtained by Nick Weir at the Palomar 60 inch telescope, shows *r*-band emission in the reflection nebulosity surrounding V1331 Cygni. At blueshifted velocities, CO (1→0) emission lies to the south and east of the star, and at redshifted velocities to the north and west. Taken together, these regions resemble an elliptical ring, 75″ × 50″ (4.1 by $2.8 \times 10^4$ AU) in size, with the semimajor axis orientated at PA ~40°. The reflection nebulosity and the CO ring emission appear similar in form with the nebula lying closer to the star. Within the ring the gas appears distributed in clumps of typical size 9″ × 5″ (5.0 by $2.8 \times 10^3$ AU). The lack of observed $^{13}$CO (1→0) ring emission limits the CO optical depth to $\tau_{CO} \leqslant 7$. We adopt a minimum excitation temperature of 10 K, as indicated by the peak brightness temperatures. Masses, calculated from Eq. (1), are 8–52 × $10^{-3}$, 6–42 × $10^{-3}$, and 1–7 × $10^{-3}\mathscr{M}_\odot$ for the blue arc, red arc, and a typical clump, respectively, in the limits of $\tau \ll 1$ and $\tau \leqslant 7$.

### 3.2 CSO Results

Emission from V1331 Cygni was detected in four molecular lines at the CSO, namely the $J = 2 \rightarrow 1$ transitions of CO, $^{13}$CO, and C$^{18}$O, and the $J = 3 \rightarrow 2$ transition of CO. Spectra, corrected for main beam efficiencies, are displayed in Fig. 4. The CO (2→1) peak brightness temperature, $T_{MB} \sim 4.8$ K, occurs at $0.27 \pm 0.32$ km s$^{-1}$. Wing emission extends to $-10$ and $+20$ km s$^{-1}$ with a dip in the blueshifted emission occurring at $-2.2$ km s$^{-1}$. The CO (3→2) spectrum is similar, albeit weaker, with peak $T_{MB} = 3.9$ K at $0.17 \pm 0.21$ km s$^{-1}$. By contrast, the $^{13}$CO (2→1) spectrum, with peak $T_{MB} = 4.1$ K at $-0.13 \pm 0.33$ km s$^{-1}$, displays no redshifted and only weak blueshifted wing emission. $^{13}$CO (2→1) emission 15″ to the east does, however, possess a weak redshifted wing. The C$^{18}$O (2→1) spectrum shows no wing emission with the peak of $T_{MB} = 0.83$ K occurring at a comparatively lower velocity of $-1.31 \pm 0.34$ km s$^{-1}$. Relative line intensities suggest that CO and $^{13}$CO emission is optically thick in the line center but that C$^{18}$O (2→1) is optically thin, with $\tau_{C^{18}O} \sim 0.25$. The dip in CO emission, centered near the velocity of the C$^{18}$O peak, most likely arises from self-absorption. Ratios of the CO/$^{13}$CO line strength suggest that blueshifted CO (2→1) wing emission between $-4$ and $-8$ km s$^{-1}$ possesses an average optical depth $\tau_{CO} \sim 15$. As the optical depth of the redshifted wing emission is poorly constrained, we adopt a maximum $\tau_{CO} \leqslant 15$ for both wings in our outflow calculations.

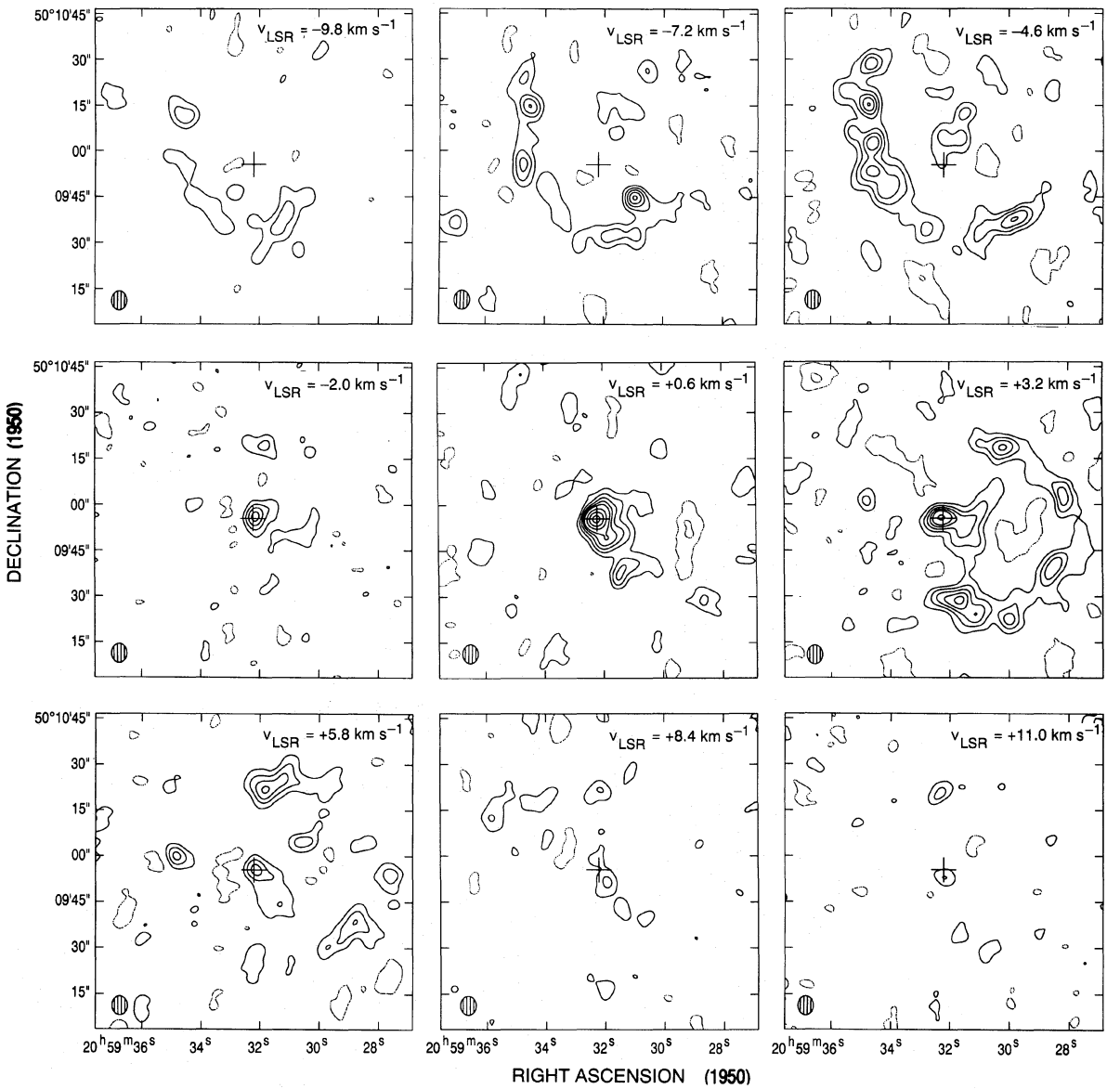


FIG. 2. Aperture synthesis maps showing the distribution of CO (1→0) emission in individual 1 MHz channels. The mean velocity for each map is shown in the top right corner. The peak flux occurs in the velocity range −0.7 to +1.9 km s$^{-1}$ and is 2.84 Jy/beam. Contours begin at, and are separated by 2$\sigma$, 0.24 Jy/beam.

CO (2→1) line emission was mapped at 10″ spacings over a region 150″×150″ centered on V1331 Cygni. At velocities between −1.0 and +1.0 km s$^{-1}$, gas is concentrated at the stellar position; strong extended emission that was resolved out by the interferometer is evident between −4.5 and +2.5 km s$^{-1}$. Emission is also seen extending radially away from the star to the northwest between −2.0 and −0.75 km s$^{-1}$ and to the south between +1.0 and +2.5 km s$^{-1}$. Significant gas structure is also present away from the cloud velocity at larger blue and redshifted velocities. Figure 5(a) shows the blueshifted emission structure at velocities between −9.5 and −4.0 km s$^{-1}$ which compares well with the arc in the CO (1→0) image [Fig. 3(a)]. Likewise, the redshifted emission between +2.0 and +6.0 km s$^{-1}$ [Fig. 5(b)] resembles the structure in Fig. 3(b). In both cases the CO (2→1) emission is stronger and more extended with total integrated fluxes of 620 Jy km s$^{-1}$ and 2000 Jy km s$^{-1}$ for the blue and red arcs, respectively. As the emission fills the beam, Eq. (4) can be used to estimate the $H_2$ mass:

$$\mathcal{M}_{H_2} = 1.42\times10^{-10} \times \frac{(T_x+0.93)}{e^{-16.76/T_x}} \frac{\tau_{CO}}{(1-e^{-\tau})} \frac{D^2_{kpc}}{X(CO)} \int S_\nu \, dv \; \mathcal{M}_\odot, \quad (4)$$

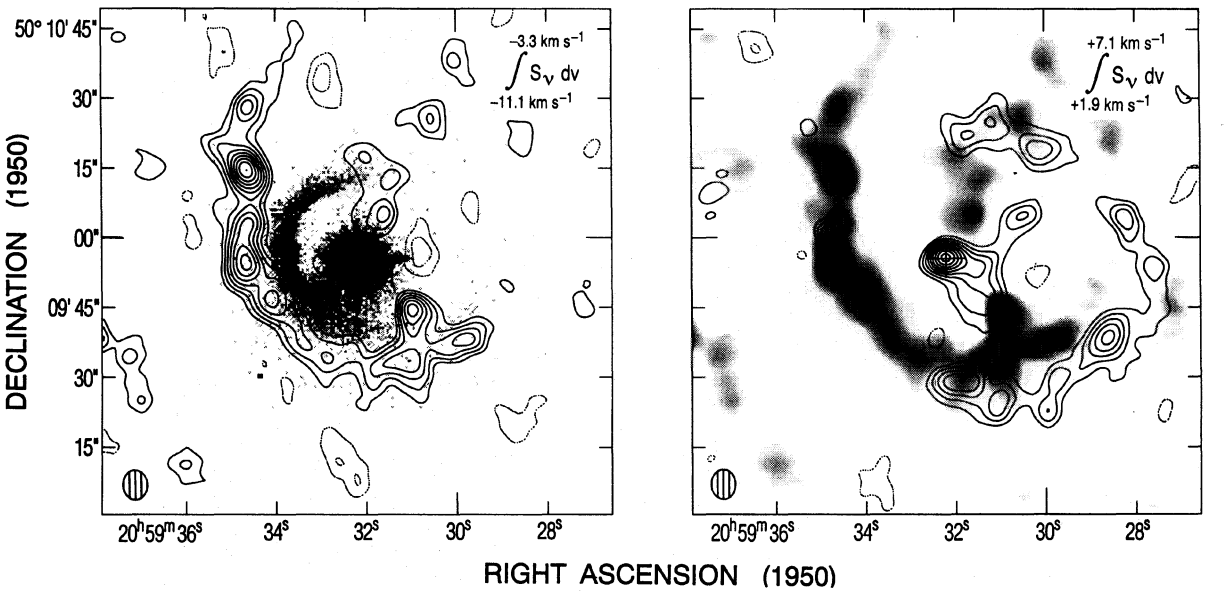


FIG. 3. Contour maps of the CO (1→0) emission integrated over the velocity ranges −11.1 to −3.3 km s$^{-1}$ (a) and +1.9 to +7.1 km s$^{-1}$ (b). Optical *r* band emission from the reflection nebulosity is depicted in greyscale in 3a. CO emission in (a) is shown as a greyscale image in (b) for comparison. The rms noise level, 1$\sigma$, is 0.50 Jy/beam km s$^{-1}$. Contours are at 20%, 30%, 40%, 40%, 50%, 60%, 70%, 80%, and 90% of the peak flux, 6.7 Jy/beam km s$^{-1}$.

where parameters are as described for Eqs. (1)–(3). For an excitation temperature of 10 K and $1 > \tau_{CO} \leqslant 15$, we calculate masses of $16\text{–}230 \times 10^{-3}$ and $50\text{–}310 \times 10^{-3} \mathcal{M}_\odot$ for the blue and redshifted emission depicted if Figs. 5(a) and 5(b). Comparison of the derived masses suggests the interferometer resolved out more than 85% of the single dish flux in the red arc, but less than 50% in the blue arc.

## 4. DISCUSSION

### *4.1 The Central Source*

Models of the far-infrared and submillimeter spectral energy distribution of V1331 Cygni are consistent with the presence of a circumstellar accretion disk (Weintraub *et al.* 1991). Our longer wavelength continuum measurements can further constrain the disk parameters. Following Beckwith *et al.* 1990, our observations together with those from Weintraub *et al.* and the *IRAS* satellite were modeled as emission arising from a radially averaged disk. We fit power law dependences for density ($p=1.5$) and temperature ($q=0.49$) over a radius range of 0.055 to 125 AU and find a disk mass of $\mathcal{M} = 0.50 \pm 0.15 \mathcal{M}_\odot$ with emissivity index $\beta = 1.0 \pm 0.2$, assuming a temperature at the disk's inner radius of 1500 K. Our fit to the spectral energy distribution is shown in Fig. 6 together with that of Wein-

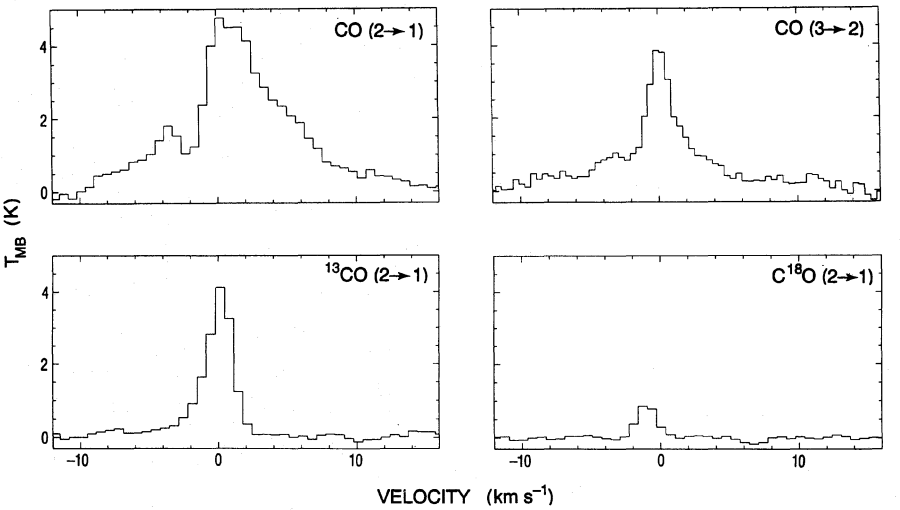


FIG. 4. Line emission in CO (2→1), CO (3→2), $^{13}$CO (2→1), and C$^{18}$O (2→1), as detected at the CSO. Temperatures have been corrected for main beam efficiencies.

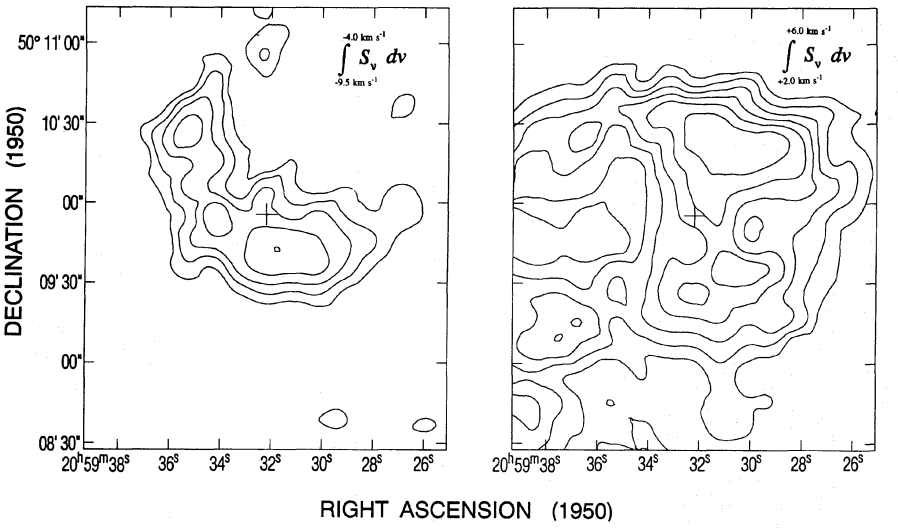


FIG. 5. Maps of the CO (2→1) emission observed at the CSO integrated over the velocity ranges −9.5 to −4.0 km s$^{-1}$ (a) and +2.0 to +5.0 km s$^{-1}$ (b). Contours are separated by 10% of the peak flux, 10.9 K km s$^{-1}$, and begin at 30% in (a) and at 50% in (b).

traub *et al.* which predicts higher fluxes at lower frequencies. We stress, however, that absolute disk mass estimates are only accurate to within an order of magnitude and are sensitive to the assumed mass opacity (Draine 1989; Beckwith *et al.* 1990; Beckwith & Sargent 1991). For example, Weintraub *et al.* use a mass opacity $\kappa_0=2.0$ cm$^2$ g$^{-1}$ at 350 $\mu$m, while here we adopt 0.1 cm$^2$ g$^{-1}$ at 250 $\mu$m (Beckwith & Sargent 1991). However, providing the mass opacity does not vary significantly with evolutionary state, our result of $\mathcal{M}=0.5\pm0.15$ implies a disk relatively more massive than those found around classical T Tauri stars (HL Tau$\sim0.1\mathcal{M}_\odot$) using the same model.

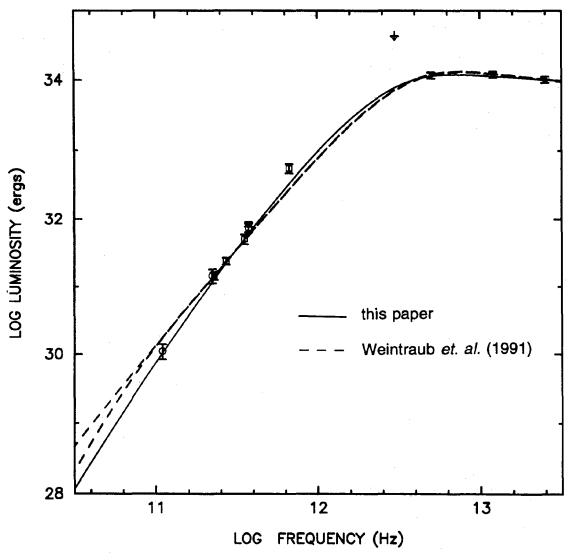


FIG. 6. The spectral energy distribution of V1331 Cygni with our model disk fit depicted with a solid line. Also shown with a broken line is the range of fit from Weintraub *et al.* (1991). Data points shown are those from *IRAS*, Weintraub *et al.* (1991), and this paper in the frequency limits $10^{12}$ to $10^{13.5}$, $10^{11.4}$ to $10^{12}$, and $10^{11}$ to $10^{11.4}$ Hz, respectively.

In Figs. 1(a)–1(c), a gaseous envelope, $\sim6000\times4400$ AU in size, mass $\geqslant0.32\mathcal{M}_\odot$, is centered near the stellar position. If distributed spherically, this envelope produces a visual extinction toward V1331 Cygni of $\geqslant21^m$, larger than the observed $A_v=2.4$, suggesting the gas lies in a flattened structure. This molecular disk or envelope appears smaller (2750×2200 AU) when seen in $^{13}$CO (2→1) emission, possibly because the smaller beam resolves out more extended emission. Excitation effects may also localize the emission nearer the star. The CO (1→0) and CO (2→1) maps suggest that, in the stellar vicinity, the line core emission in single dish spectra (Fig. 4) arises from this envelope. Emission peaks at higher velocities as the optical depth of the transition increases, suggesting collapse. However, in the optically thick CO (2→1) spectrum, redshifted wing emission is dominant, indicative of outflow (Zhou *et al.* 1993).

### *4.2 Bipolar Outflow*

Two linear structures, best seen in the interferometer maps in Fig. 2 but also detected at the CSO, extend radially away from V1331 Cygni. Blueshifted CO (1→0) and CO (2→1) emission is present to the northwest of V1331 Cygni between velocities of −8.7 to −0.75 km s$^{-1}$. Redshifted gas is also evident to the southwest but is not fully mapped. Previous CO (2→1) studies (Levreault 1985), with larger spatial coverage, delineate the flow structure more completely. Together these two components form a bipolar outflow with its axis between PA 140° and 230°. The low optical extinction ($A_v=2.4$) toward V1331 Cygni suggests the star lies on the near side of its parent molecular cloud (Anglada *et al.* 1989). The blueshifted outflow

may be weak as it has broken out of the cloud, while its redshifted counterpart propagates into the cloud, sweeping up comparatively more mass, facilitating detection. This suggests that V1331 Cygni is viewed more along its outflow axis than in the plane of the sky.

### *4.3 Ring Emission*

We detect a gaseous ring around V1331 Cygni $4.1\times10^4$ by $2.8\times10^4$ AU in size, with a maximum velocity dispersion of $\sim20$ km s$^{-1}$. Conservative estimates suggest a ring mass of at least $0.07\mathcal{M}_\odot$ and possibly up to $0.54\mathcal{M}_\odot$. At these distances and velocities, it is unlikely that the emission is from infalling material. The observed emission pattern [Figs. 2, 3(a), and 3(b)] cannot arise from rotating gas, as the angular momentum would be large and the implied velocity gradient of $\sim120$ km s$^{-1}$ pc$^{-1}$ would be much larger than typical cloud core values of $\sim10$ km s$^{-1}$ pc$^{-1}$ (Goldsmith & Arquilla 1985; Myers 1985). We believe the emission arises from outflowing material. However, the observed spatial dependence of emission with velocity cannot be produced by a bipolar outflow or a uniformly expanding spherical shell (see Bachiller & Gomez-Gonzalez 1992, and references therein).

A simple model of an optically thick, radially expanding torus, radius $\sim1.7\times10^4$ AU, crudely reproduces the observed distribution of emission. The orientation of the torus, major axis position angle $\sim40°$ inclined at 30° to the plane of the sky, was deduced from comparison with the integrated CO (1→0) ring emission detected by the interferometer. We then determined the radial expansion velocity of the torus by modeling the high velocity resolution CO (2→1) data obtained at the CSO.

Channel maps of the CO (2→1) blue arc emission between $-8.75$ and $-4.75$ km s$^{-1}$, averaged to a velocity resolution of 0.5 km s$^{-1}$, are shown in contours in Fig. 7. Emission is concentrated toward PA 130° at high velocities and is more extended at lower velocities. Model results for a torus, height $\sim8\times10^3$ AU, width $\sim2\times10^3$ AU, expanding at 22 km s$^{-1}$, are depicted in greyscale. The model emission is normalized to unity for each channel as detailed radiative transfer calculations were not conducted. The asymmetry of the torus, possible evidence of influence by the surrounding ambient cloud, causes discrepancies between the data and the model fit. We also note that the aspect ratio is poorly constrained by the low spatial resolution. Nevertheless, the model faithfully predicts the trends in emission distribution although it overestimates the extent of the high velocity emission. We therefore suggest that V1331 Cygni is surrounded by a torus, radius $\sim1.7\times10^4$ AU, expanding at $\sim22\pm4$ km s$^{-1}$, implying an implantation time of $\sim4\times10^3$ yr at the current expansion rate.

### *4.4 Torus Formation Mechanisms*

To sweep up the V1331 Cygni torus by radiation pressure requires a stellar luminosity over the torus lifetime of $\geqslant10^4L_\odot$, much greater than the present value of $\sim53L_\odot$. Theoretical models of rapidly rotating protostars can produce circumstellar rings, but not on the spatial scales observed here (Williams & Tohline 1988). Therefore the torus is probably wind-driven molecular gas. The torus structure most likely mimics the original gas distribution rather than the wind geometry, for a planar wind though possible is unlikely. As stars form, angular momentum conservation causes accreting material to be concentrated toward the equatorial plane where a more isotropic wind may sweep up gas to form the torus. The torus may therefore be considered as part of an incomplete shell. Indeed, the circular reflection nebulosity may trace the inner edge of an evacuated cavity. Since the torus inclination is $\sim30°$, V1331 Cygni is viewed more pole-on, in agreement with the orientation deduced from the bipolar outflow, and with the suggestion that moderately extincted FUors are observed along the system poles (Kenyon & Hartmann 1991).

The torus possesses a momentum between $\sim1.5\rightarrow11.9\mathcal{M}_\odot$ km s$^{-1}$. To sweep up the torus requires a mass loss rate between $1.0\rightarrow8.0\times10^{-6}\mathcal{M}_\odot$ yr$^{-1}$ over its lifetime, assuming a wind velocity $v_{\rm wind}=370$ km s$^{-1}$ (Mundt 1984). As the torus in our model only subtends $\sim0.4\pi$ steradians, the required mass loss rate may be substantially higher for an isotropic wind. The current mass loss rate of $\dot{\mathcal{M}}\leqslant10^{-6}\mathcal{M}_\odot$ yr$^{-1}$ is therefore insufficient to drive the outflow implying the torus formed at an earlier, more vigorous, stage. Since V1331 Cygni is a FUor pre-outburst candidate, and the FUor phenomenon is possibly repetitive, the torus may have resulted from a previous outburst. For a typical FUor event lasting $\sim100$ yrs (Hartmann 1992), with $\dot{\mathcal{M}}\sim10^{-5}\mathcal{M}_\odot$ yr$^{-1}$ and $v_{\rm wind}=370$ km s$^{-1}$ (Croswell *et al.* 1987; Mundt 1984), a total of $0.4\mathcal{M}_\odot$ km s$^{-1}$ can be entrained by a momentum conserving stellar wind. For the T Tauri star, V1331 Cygni is moderately massive, lying between the classical T Tauri stars and the Herbig Ae and Be stars in the Hertzsprung–Russell diagram (Chavarria 1981); the distance and $A_v$ adopted here imply $M_{\rm pg}=1^{\rm m}$, significantly higher than usual for FUors. The outburst may therefore have been even more energetic than average. Clearly, torus formation requires either a single, very vigorous outburst or a series of multiple outbursts; we suggest the torus may be a relic from a younger state of very energetic activity, possibly when V1331 Cygni was more embedded. The torus expansion time, $\sim4\times10^3$ yr, is thus an upper limit to the time between successive outbursts and is similar to Herbig's (1989) estimate of $5\times10^3$ yr.

Such an energetic mass loss stage will have considerable effects on the ambient cloud and possibly serious, although unknown, effects on the circumstellar disk. An isotropic wind would impart $\geqslant10^{45}$ ergs into the surrounding cloud, comparable to that deposited by bipolar outflows (Beckwith *et al.* 1983), but over a larger angular extent. Although subsequent outbursts may have decreasing effect on the cloud, repeated outbursts may impart $\geqslant10^{47}$ ergs. This more isotropic form of mass loss suggests FUor outbursts, or their precursors, may considerably change the energy

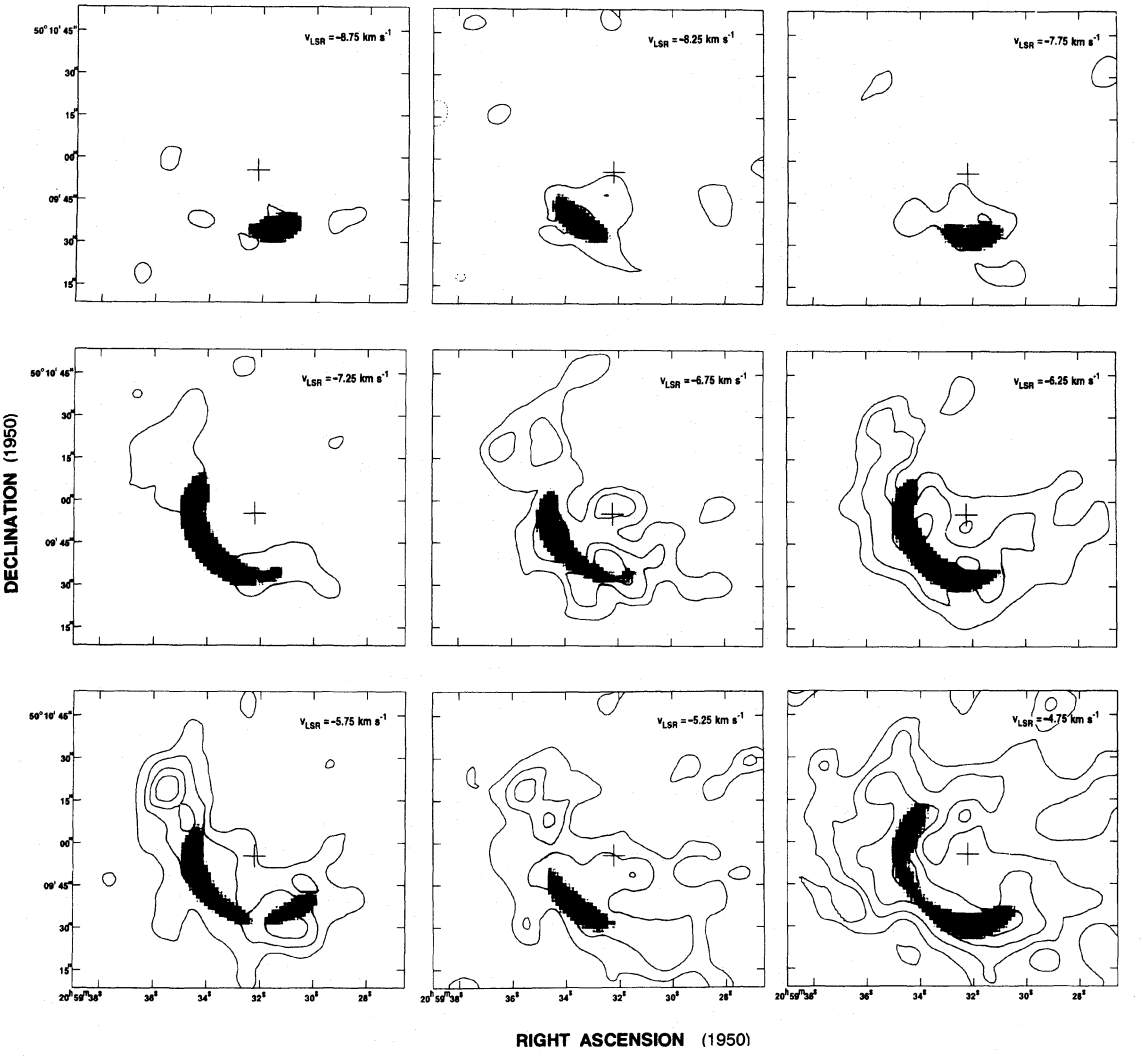


FIG. 7. Maps of the CO (2→1) emission observed at the CSO between −8.75 and −4.75 km s$^{-1}$. The mean velocity for each map is shown in the top right corner. Contour levels begin at the 4$\sigma$ level, 0.8 K, and are separated by 0.4 K (2$\sigma$). The optimal model fit torus is depicted in greyscale.

and momentum input to the ambient cloud and that their role has been previously underestimated.

## 5. CONCLUSIONS

The FU Orionis pre-outburst candidate, V1331 Cygni, is surrounded by a massive $0.5 \pm 0.15 \mathcal{M}_\odot$ circumstellar disk. Surrounding this is a flattened envelope of gas, $\sim 10^4$ AU in diameter, mass $\geqslant 0.32 \mathcal{M}_\odot$ which is in turn surrounded by a nearly circular reflection nebula. At larger scales, we observe both blue and redshifted outflow components of a previously undetected bipolar outflow, whose relative strengths imply V1331 Cygni is viewed more pole-on.

The most striking outflow feature is a large molecular torus surrounding V1331 Cygni, 4.1 by $2.8 \times 10^4$ AU in size, mass 0.07–0.54$\mathcal{M}_\odot$, expanding at $22 \pm 4$ km s$^{-1}$ in the system's equatorial plane. The blueshifted component of the torus expands away from the cloud center; it is well defined due to the minimal confusion by emission from foreground gas as indicated by the fine structure of the associated reflection nebula. The redshifted component expands into the densest regions, is more massive, and appears more extended. We suggest the torus was swept up by a roughly isotropic wind $\sim 4 \times 10^3$ yr ago. The outflow energetics require a high mass loss rate, possibly a FUor outburst, which deposited some $\geqslant 10^{45}$ ergs into the ambient cloud. This may be the first direct observational evidence for the repetitive nature of the FU Orionis phenomenon.

We are indebted to the staff of the Owens Valley millimeter-wave array and the Caltech Submillimeter Observatory for their unfailing support, and extend special

thanks to Taco for his assistance with the CSO mapping software. We are grateful to N. Weir and J. Eislöffel for kindly supplying optical images. S. M. thanks D. Koerner for many illuminating and stimulating discussions and for supplying the SED code. Astronomy with the Owens Valley Array is funded by NSF Grant No. AST 90-16404 and the CSO by NSF Grant No. AST 90-15755. S. M. is supported by NASA Grant Nos. NAGW-3172 and NAGW-2297, part of the Origins of Solar Systems Research Program.

## REFERENCES

Anglada, G., Rodriuez, L. F., Torrelles, J. M., Estalella, R., Ho, P. T. P., Canto, J., Lopez, R., & Vendes-Montenegro, L. 1989, ApJ. 341, 208
Bachiller, R., & Gomez-Gonzalez, J. 1992, A&AR, 3, 257
Beckwith, S., Natta, A., & Salpeter, E. E. 1983, ApJ, 267, 596
Beckwith, S. V. W., & Sargent, A. I. 1991, ApJ, 381, 250
Beckwith, S., Sargent, A. I., Chini, R. S., & Gusten, R. 1990, AJ, 99, 924
Calvet, N., Hartmann, L., & Kenyon, S. J. 1991, ApJ, 383, 752
Carr, J. S., Harvey, P. M., & Lester, D. F. 1987, ApJ, 321, 71
Chackerian, C., & Tipping, R. H. 1983, J. Mol. Spectrosc., 99, 431
Chavarria-K., C. 1981, A&A, 101, 105
Croswell, K., Hartmann, L., & Avrett, E. H. 1987, ApJ, 312, 227
Draine, B. T. 1989, Proceedings of the 22 ESLAB Symposium on Infrared Spectroscopy in Astronomy, edited by B. H. Kaldeich (ESA Publications, Noordwijk)
Ellison, B. E., & Miller, R. L. 1987, Int. J. Infrared and Millimeter Waves, 8, 608
Ellison, B. E., Schaffer, P. L., Schaal, W., Vail, D., & Miller, R. E. 1989, Int. J. Infrared and Millimeter Waves, 10, 937
Eislöffel, J., Hessman, F., & Mundt, R. 1990, A&A, 232, 70
Goldsmith, P. F., & Arquilla, R. 1985, in Protostars and Planets II, edited by D. C. Black and M. S. Matthews (University of Arizona, Tucson)
Hartmann, L. 1992, in NATO ASI on The Formation and Evolution of Stars, edited by N. Kylafis and C. Lada
Hartmann, L., & Kenyon, S. J. 1985, ApJ, 299, 462
Hartmann, L., & Kenyon, S. J. 1987, ApJ 312, 243
Hartmann, L., Kenyon, S. J., & Hartigan, P. 1993, in Protostars and Planets III, edited by E. H. Levy and J. I. Lunine (University of Arizona, Tucson)
Herbig, G. H. 1958, ApJ, 128, 259
Herbig, G. H. 1977, ApJ 217, 693
Herbig, G. H. 1989, in ESO Workshop on Low-Mass Star Formation and Pre-Main Sequence Objects, edited by B. Reipurth (ESO, Garching), 233
Herbig, G. H., & Robbin Bell, K. 1988, Lick Ob. Bull. 1111
Kenyon, S. J., & Hartmann, L. 1991, ApJ, 383, 664
Langer, W. D., & Penzias, A. A. 1993, ApJ, 408, 539
Levreault, R. M. 1985, Ph.D. thesis, University of Texas at Austin
Levreault, R. M. 1988, ApJ, 330, 897
Mundt, R. 1984, ApJ, 280, 749
Mundt, R., Stocke, J., Strom, S., Strom, K., & Anderson, E. 1985, ApJ, 297, L45
Myers, P. C. 1985, in Protostars and Planets II, edited by D. C. Black and M. S. Matthews (University of Arizona, Tucson)
Petrov, P. P., & Herbig, G. H. 1992, ApJ, 392, 209
Reipurth, B. 1990, IAU Symposium No. 137, 229
Scoville, N. Z., Sargent, A. I., Sanders, D. B., Claussen, M. J., Masson, C. R., Lo, K. Y., & Phillips, T. G. 1986, ApJ, 303 416
Shevchenko, V. A., Yakubov, S. D., Ambaryan, V. V., & Garibdzhanyan, A. T. 1991, Sov. Astronomy-A.Zh., 35(2), 135
Staude, H. J., & Neckel, Th. 1991, A&A, 244, L13
Wachmann, A. A. 1939, Beob. Zirk., 21:12
Weintraub, D. A., Sandell, G., & Duncan, W. 1991, ApJ, 382, 270
Welin, G. 1976, A&A, 49, L145
Welty, A., Strom, S., Edwards, S., Kenyon, S. J., & Hartmann, L. 1992, ApJ, 397, 260
Williams, H. A., & Tohline, J. E. 1988, ApJ, 334, 449
Zhou, S., Evans II, N. J., Kömpe, C., & Walmsley, C. M. 1993, ApJ, 404, 232